Computers & Structures Vol. 44, No. 4, pp. 699–716, 1992
Printed in Great Britain.

0045-7949/92 $5.00 + 0.00
Pergamon Press Ltd

THREE-DIMENSIONAL FINITE-ELEMENT MODELLING OF NORMAL- AND HIGH-STRENGTH REINFORCED CONCRETE MEMBERS, WITH SPECIAL REFERENCE TO T-BEAMS

S. M. Seraj,† M. D. Kotsovos‡ and M. N. Pavlović§

†Department of Civil Engineering, Imperial College, University of London, U.K.

‡Department of Civil Engineering, National Technical University of Athens, Greece

§Department of Civil Engineering, Imperial College, University of London, London SW7 2BU, U.K.

(*Received* 27 *February* 1991; *revised* 9 *May* 1991)

Abstract—A three-dimensional finite-element model for structural concrete, based on brittle constitutive relationships at the material level, is applied to the analysis of reinforced-concrete members. The generality of the 'constant-parameter' finite-element model, previously established for normal-strength concretes, is now extended to high-strength mixes. Emphasis is placed on the modelling of T-beams (encompassing both ranges of concrete strength), for which results from laboratory tests by the authors are available; and, in addition, a high-strength rectangular member is also considered, its testing having been carried out by other workers. Not only is there a general scarcity of reported experimental data for high-strength concrete components but, to the authors' knowledge, no attempt to apply finite-element modelling to this higher range of concrete strengths seems to exist in the literature. The analysis of the various structural components is preceded by the modelling of a particular, normal-strength T-beam, which is studied by adopting a number of mesh discretizations in order to accomplish an economical solution without impairing the accuracy of the numerical predictions. What emerges from the present investigation is that the existing finite-element model, applied in the past to normal-strength concretes, is just as applicable to high-strength mixes. In fact, it appears that the latter type of concrete is even more amenable to simple modelling of complex reinforcement detailing, and a likely explanation for this trend is put forward on the basis of the differing degree of 'triaxiality' between normal- and high-strength concretes.

INTRODUCTION

Widespread usage of the finite element (FE) method in the analysis of reinforced-concrete (RC) members designed in accordance with the currently prevalent ultimate limit-state philosophy is largely precluded by the notorious lack of generality of nonlinear FE models for structural concrete [1, 2]. Such shortcomings as regards applicability to arbitrary structural components are usually combined with the need to deal with several material input parameters, some of which are not readily obtainable and/or need to be varied with problem type. Nevertheless, the recent development of a fully three-dimensional (3-D) FE package [1–3]—an extension of an earlier 2-D model [4, 5]—appears to be capable of reliable predictions irrespective of structure type, even though the material properties (i.e. both the constitutive relations and the failure criteria) are reduced to the specification of the most basic parameter, namely the cylinder strength f_c, the assessment of which is both straightforward and reliable. However, whereas this model has been thoroughly validated against a wide range of experimental data pertaining to normal-strength concrete, no case studies involving high-strength concrete mixes have, so far, been tackled. In fact, it would appear that such high-strength structural members have not formed part of any previous modelling investigation, whether two- or three-dimensional. It is important to note that, in the present research, 3-D analysis has been considered mandatory since the complicated geometry and reinforcement details of the T-beams studied cannot be reduced to 2-D treatment. Moreover, the triaxial conditions prevalent in the members investigated can be better catered for by a 3-D analysis.

The present paper aims at extending the generality of the 3-D model so as to encompass also high-strength components. This is done primarily by reference to the analysis of a series of T-beams, for which the authors also possess the relevant experimental data covering both normal- and high-strength mixes. In addition, the case study of a high-strength rectangular beam is also presented, as this specimen represents one of the fairly rare instances of reported test data pertaining to high-strength concrete members and, as such, is clearly useful in assessing whether the generality of the 3-D FE package also extends to such concrete mixes.

The main features of the 3-D FE model, and its related objectivity studies have been described in sufficient detail elsewhere [1–3] and, thus, it will be sufficient to simply recall the recommendations stemming from these references as regards the optimum

strategies to be adopted for successful numerical analysis. The concrete is modelled by means of a 20-node serendipity element HX20, where the modelling of the steel reinforcement is based on a three-node parabolic element LM03 having only axial stiffness. The numerical integration of the brick element HX20 is carried out by means of the $2 \times 2 \times 2$ Gaussian-integration rule; similarly, for element LM03, the integration is carried out at two Gauss points. It should be noted that, in the present modelling, the steel elements must coincide with the edges of the serendipity element, because the HX20 elements cannot allow a more flexible distribution of steel bars due to the absence of mid-face and centre nodes (unlike the Langrangian element [1–3], which will not be used in the present study). When concrete cracks, there is a reduction in shear moduli across the plane of the crack, and it is usual to define these by multiplying their uncracked values by the shear-retention factor (SRF), a parameter that is clearly associated with the concept of 'aggregate interlock'; as argued elsewhere [1, 4], the effect of aggregate interlock on the load-carrying capacity of a member is insignificant, and this is consistent with the chosen (constant) SRF ($=0.1$), a value which, at the same time, is also sufficient to ensure the necessary numerical stability [1]. In the analyses, 'dowel action' is disregarded and perfect bond between concrete and steel asumed. Cracking is mimicked through smeared modelling, while 'strong' nonlinearities are best accounted for through the iterative method known as the 'Newton–Raphson plus' technique. As mentioned earlier, only the value of the uniaxial cylinder compressive strength needs to be input to describe truly the properties of the relevant concrete mix, while the steel response is defined upon specification of the yield- and ultimate-stress values.

Although the plotting convention has been described in detail elsewhere [1, 3], it is helpful to briefly summarize it at this point. Plots are superimposed onto the mesh lying on a plane parallel to the reference plane (XZ). The symbols for the various cracks at the relevant Gauss points are as follows. Oriented dashes represent the intersection of a crack plane with the plotting plane XZ whenever the angle subtended between these two planes exceeds 45°. Should both planes form an angle smaller than 45°, the crack plane is indicated by a circle. Three cracks at the same Gauss point are indicated by an asterisk. Displacement shapes at the various load levels can be suitably magnified, and the appearance of very large and/or distorted shapes helps to identify quickly the onset of a mechanism (whether real or numerical in nature); the latter is especially relevant for load step '777' plots that relate to the last performed iteration in an analysis. [In the present work, a magnification factor of 5 is usually adopted, except for some of the load step '777' plots (and, sometimes, that of its preceding load step), for which deflections become quite large so that, for purposes of clarity, they were not magnified.] Finally, it should be remembered that, in all instances, the maximum sustained load (MSL) is taken to represent failure, even though the MSL corresponds to the last converged load step. Load step '777' (corresponding to the MSL plus an additional load-step increment), if shown, is for reference only.

ECONOMIC MODELLING OF REINFORCED CONCRETE BEAM

Scope

The purpose of this preliminary study is to model the same structural form by adopting different mesh configurations. In this respect, it should be recalled that the usual notion of convergence to the correct solution through mesh refinement is not meaningful, as the material chracteristics are derived from a cylinder test which is sufficiently large to enable the *average* properties of what is really a heterogeneous mix to be established. For this reason, it is unrealistic to adopt finite elements that are smaller than about three times the maximum size of aggregate used in the particular concrete mix [5]. Such thinking also helps control the size of the structural stiffness matrices which increase rapidly with mesh refinement due to the large number of degrees of freedom per brick element. It is important to note that the coding of the present model has been written in FORTRAN 77 in a medium-range computer, Masscomp MC5400, with its inherent limitations of memory and speed. The biggest structural component modelled and analysed previously in this system was a 3200 mm long T-beam using 50 under-integrated 20-node brick elements for concrete and 104 three-node bar elements for the reinforcement [2, 6]. Details of this beam will be given later. Since the modelling of prestressed-concrete (PSC) structural forms, having sizes much larger than its reinforced counterparts, is within the scope of an ongoing research at Imperial College [7], simplifications in both geometry and reinforcement (in an effort to keep computational requirements within sensible limits and to conform to resource constraints) is deemed essential, though the present FE model is fully capable of handling the true geometry of any large member. As the PSC members to be studied in the above-mentioned research will have sections similar to the under-reinforced T-beam studied in [2, 6], it seems prudent to investigate the behaviour of the latter beam by representing it with fewer finite elements, in an attempt to obtain a mesh which leads to economic modelling without compromising the accuracy of numerical predictions. The results obtained from the study of PSC members will be reported in a future publication.

Details of the beam studied

The structural element used in the present economic-modelling study is an under-reinforced T-beam

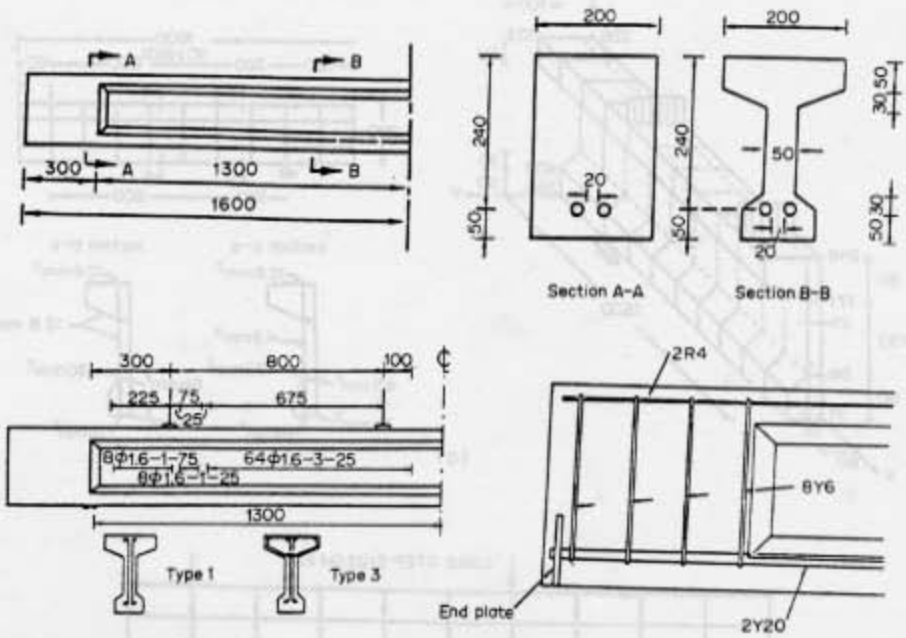

Fig. 1. Under-reinforced T-beam used for economic-modelling purposes (beam C [8]). Dimensions and reinforcement detailing.

with stirrups subjected to four-point loading, tested and reported by Kotsovos and Lefas [8]. Figure 1 summarizes the experimental details of the beam. The beam had a flexural span of 2600 mm, with an effective depth of 240 mm and overhangs of 300 mm beyond each support. The member was just under-reinforced, since the percentage of tension steel referred to the effective depth was 2.75% while the corresponding balanced percentage was 3.2%. The web reinforcement comprised 2 ⌀ 1.6 vertical legs (shown as type 1 reinforcement in Fig. 1) spaced at 75 mm from the support to the first load point, and at 25 mm from the latter up to a distance of 100 mm to the right of the second point-load (hence the web reinforcement ratios, $A_w/s\,b_w$, were equal to 0.11 and 0.32, respectively). In addition, flange stirrups, comprising a 1 ⌀ 1.6 bar (shown as type 3 reinforcement in Fig. 1) spaced at 25 mm, were provided from a distance of 125 mm to the right of the first point-load up to a length of 100 mm to the right of the second point-load (see Fig. 1). The main feature of the beam, which failed at a load of 240.1 kN, was that it attained its full flexural capacity (about 80 kN m) in spite of the high shear forces acting along the element and the low amount of web reinforcement. It is worth mentioning that the member was designed in compliance with the concept of the compressive-force path and that the design details were significantly different from those specified by current code provisions. The concrete cube strength was 40 MPa, while the yield- and ultimate-stress values of the main tension steel were 500 and 670 MPa, respectively.

Modelling using 50 brick elements

As mentioned earlier, in the previous modelling of the beam [2, 6], a mesh comprising 50 brick elements for the concrete and 104 uniaxial elements for the reinforcement (see Fig. 2a) was adopted (only one-fourth of the member was analysed due to the relevant symmetries). Certain minor changes for both the actual dimensions of the span and the position of the loads were introduced so as to use a regular mesh: thus the distance to mid-span is 1280 instead of 1300 mm, the distance from the support to the first load-point is 320 instead of 300 mm, and the half-length in pure flexure is 160 instead of 200 mm. As regards the tension reinforcement, it was 'smeared' to neighbouring brick edges in order to avoid two additional rows of brick elements (i.e. 20 HX20 more elements); nevertheless, since the total steel area and the effective depth were equal to those of the actual beam, this deviation from the test could only play a secondary role. More significant deviations from the test were introduced in the modelling of the transverse reinforcement: first, the area of the transverse bars was adjusted so as to keep the same area per unit length as in the test, but the spacing of 160 mm in the analysis was substantially higher in comparison to the spacing in the test (75 and 25 mm); and, secondly, the analysis ignored any transverse reinforcement to the right of the central point-load. A further simplification in the modelling refers to the deviation from the actual cross-section near the support, as the end block of the beam was completely ignored.

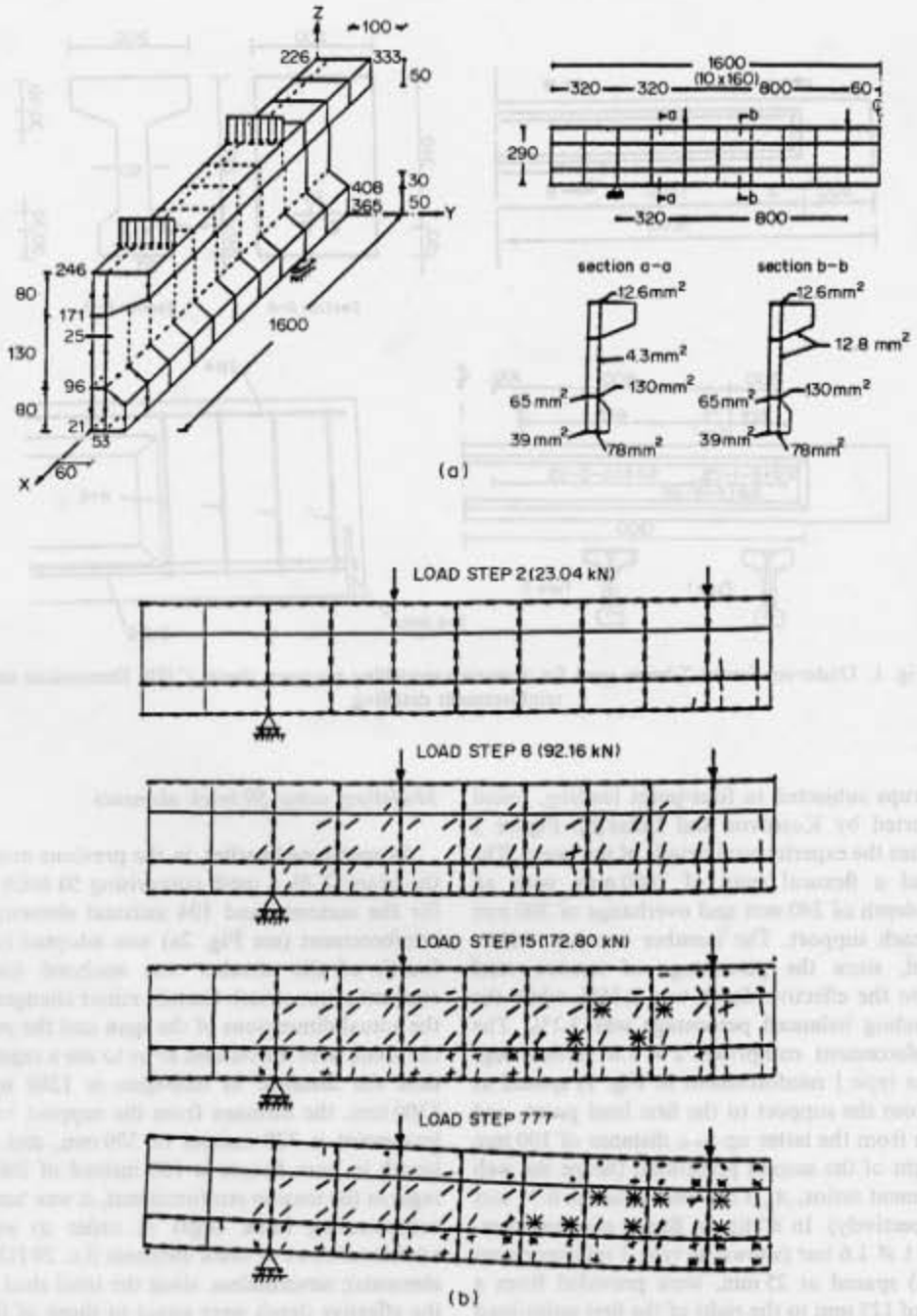

Fig. 2. Under-reinforced T-beam: (a) mesh of 50 brick elements [1]; (b) crack patterns at various load levels up to failure. (Due to symmetry only one-fourth of the beam is analysed. The position of the steel elements is indicated by dashes.)

The predicted MSL (172.8 kN) amounts to 72% of the experimental failure load (the load at which divergence occurs (184.32 kN) represents 77% of the true ultimate value). Figure 2(b) shows the analytical crack pattern at the appearance of the first flexural crack (23.04 kN), the middle load step (92.16 kN), the MSL (172.80 kN) and load step '777'. At the MSL, the stress of the tension reinforcement within the flexural span was almost at the yield value of the material. A comparison between experimental and numerical load–deflection curves may be seen in Fig. 3.

Modelling using 40 brick elements

The discretization of the under-reinforced T-beam with fewer brick elements was achieved by simplifying the geometry of the bottom flange. Figure 4 shows the FE mesh used. Such a mesh comprises 40 brick elements for the concrete and 104 uniaxial bar elements for the reinforcement (again, for one-fourth

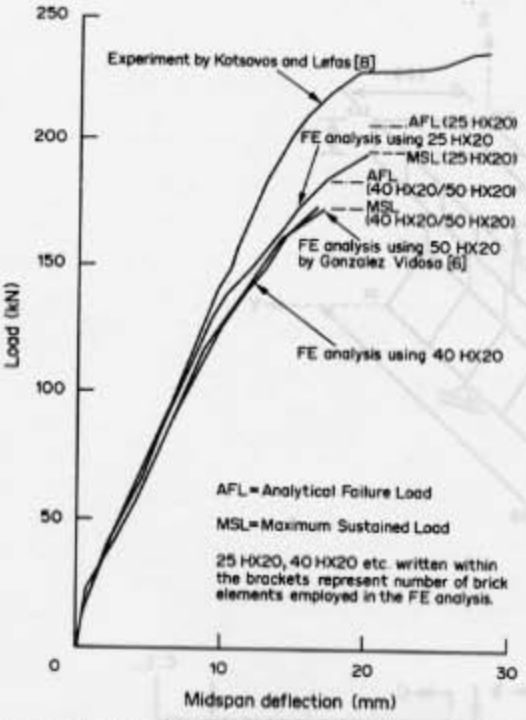

Fig. 3. Under-reinforced T-beam. Comparison between experimental and analytical load–deflection curves.

of the beam). The minor changes in the actual dimensions of the span and the position of the loads described in the previous section were kept in the present analysis in order to use a regular mesh and to ensure consistency in the interpretation of the results. It can be seen in Fig. 4 that the bottom flange has been modelled by using only 10 brick elements (instead of 20). To achieve this reduction, the shape of the bottom flange was slightly changed in the FE discretization. As regards the tension reinforcement, it was 'smeared' to the corner nodes of the neighbouring brick edges. Since the aim of this exercise was to ascertain the mesh sensitivity as regards ultimate load and overall behaviour of the structural element, no attempt was made to model the transverse reinforcement in a manner different from that adopted in the earlier 50-brick mesh.

Figure 5 shows the analytical crack pattern at different load levels up to failure. The MSL in this analysis was identical to that attained for the previous mesh, and the first flexural cracks also appeared within the flexural span at the second load step (23.04 kN). Subsequently, diagonal cracks oriented from the support to the point loads developed throughout the web of the beam (see Fig. 5 for 69.12 kN). Apart from a few additional cracks within the bottom part of the flange, the fracture process is almost stabilized up to a load level equal to 161.28 kN. At the MSL (172.80 kN), the tension reinforcement in the flexural span yielded. As for the 50-brick mesh, the divergence in the analysis was triggered by the occurrence of vertical cracks within the compressive zone of the flexural span [2]. The load–deflection curve for this analysis is practically identical to that of the earlier run (see Fig. 3). Thus, by comparing the MSLs, the crack patterns and the load–deflection curves for the 50- and 40-brick analyses, it can be concluded that a slight modification in the geometry (essentially, a reduction in the area) of a structural form below the neutral axis need not make an appreciable difference in the numerical predictions, which is in keeping with the notion espoused by the authors that cracked concrete in regions subjected to predominantly tensile-stress conditions (such as zones below the neutral axis) makes only a minor contribution to the overall load-carrying capacity of a concrete structure. Since, in the present run, the geometry of the top flange was not subjected to any modification, the region of the beam which carries compressive forces from the loading points to the support was unaffected, this being the likely reason why the modelling of the under-reinforced T-beam with a slightly smaller bottom flange gave predictions that coincide with the more refined mesh.

Modelling using 25 brick elements

The FE discretization adopted for the present analysis is shown in Fig. 6. The mesh now has only 25 under-integrated brick elements for the concrete and 77 bar elements for the steel. (Once again, one-fourth of the beam has been analysed.) A few changes in the actual dimensions of the span and the position of the loads were introduced so as to use a regular mesh. In order to simulate the experiment more closely, this mesh contains an additional brick element to model the rectangular end block in an approximate manner. The length of each brick element was 260 mm, instead of the 160 mm adopted in the previous two analyses. While the distance of the mid-span to the support was kept at 1300 mm (as in the experiment), the distance from the support to the first load-point was 260 instead of 300 mm, and the half-length in pure flexure was 260 instead of 200 mm. The length of the beam overhanging from the support was 260 instead of 300 mm. Evidently, the latter changes are unlikely to be of consequence. The geometry of the bottom flange was given a trapezoidal shape, as in the previous analysis using 40 brick elements. As regards the tension and compression reinforcement, this has been 'smeared' to the corner nodes of the neighbouring elements in such a manner that both the area of steel and the effective depth remain unchanged. The modelling of the transverse reinforcement did incorporate deviations from the test, since the amount of transverse reinforcement over the support remained the same as for the previous two runs, while the area of the transverse bars had to be re-adjusted so as to keep the same area per unit length as in the test. However, and in contrast to the two previous runs, in the present analysis, the appropriate amount of transverse

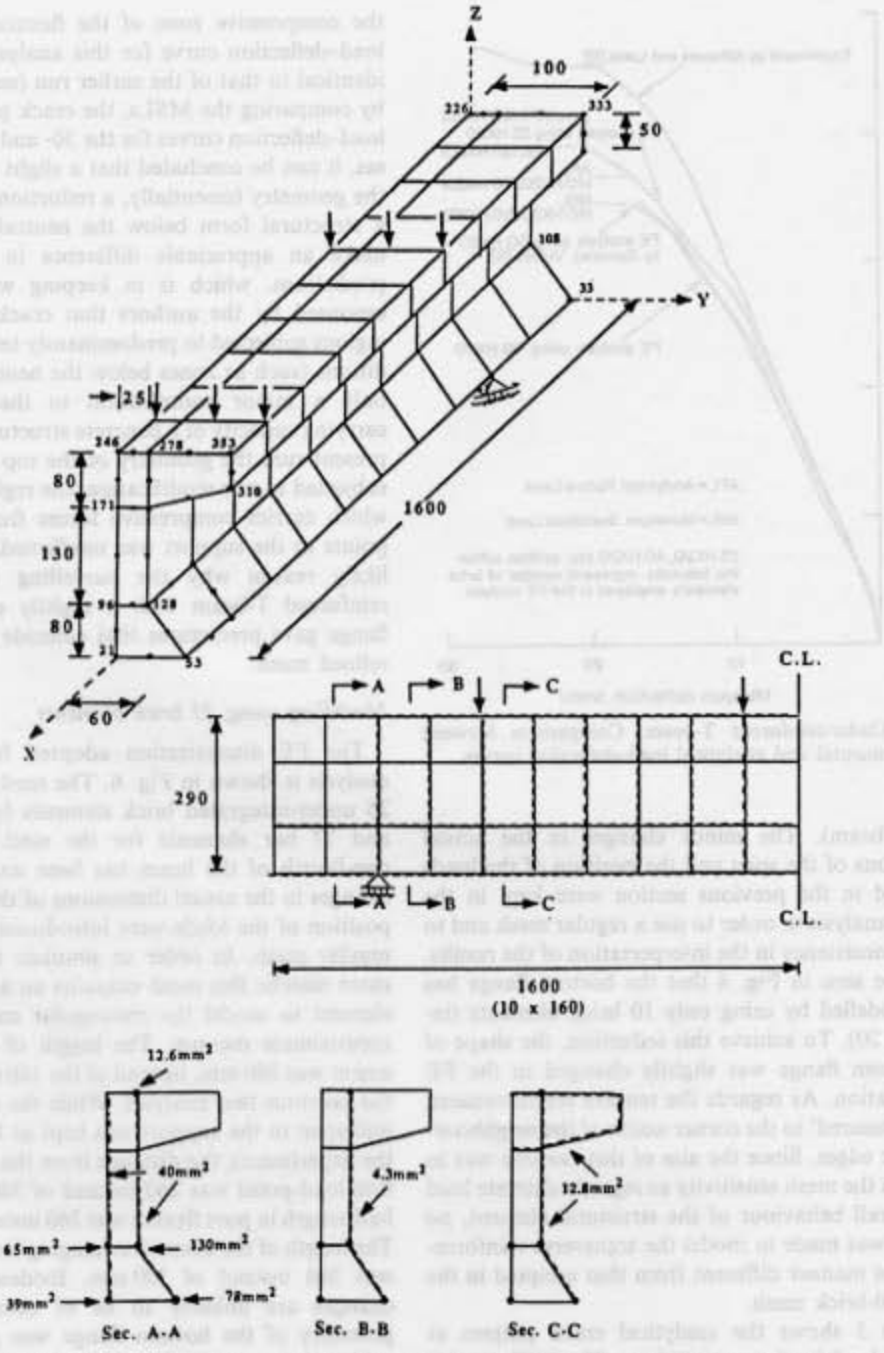

Fig. 4. Under-reinforced T-beam. Mesh of 40 brick elements. (Due to symmetry only one-fourth of the beam is analysed. The position of the steel elements is indicated by dashes.)

reinforcement was provided to the right of the central point load (i.e. in the pure-flexure span)—albeit its spacing was modelled very roughly (260 instead of 25 mm).

The MSL now becomes 195.84 kN, which is about 82% of the experimental failure load and 10% above the failure load predicted by the previous two analyses. (These percentages become 86% and 11% if the load at divergence is considered.) Figure 7 shows the analytical crack patterns at various load levels up to failure. At 23.04 kN, the first cracks appeared in the flexural span and, subsequently (at 69.12 kN), diagonal cracks oriented from the supports to the point loads develop throughout the web of the beam. The fracture process became stabilized at this stage. However, in subsequent load steps a few additional cracks were formed both at the bottom flange and near the top flange in between the load-points. At 161.28 kN, further cracks propagated into the top flange, and the web between load points was severely cracked as well.

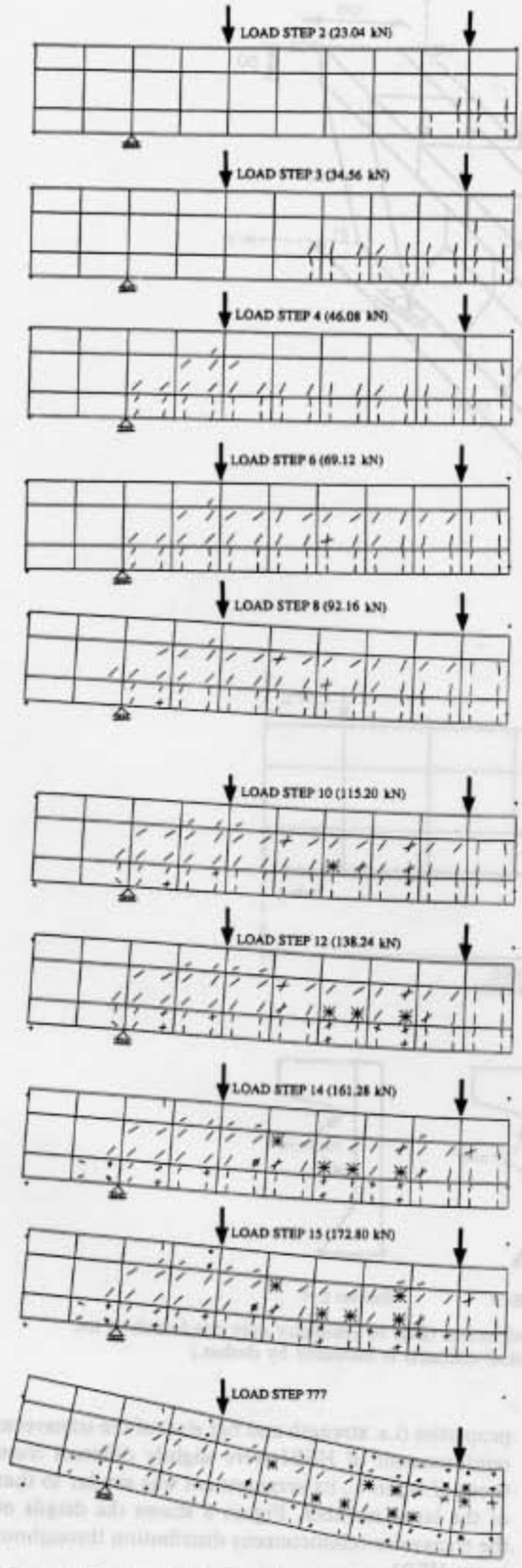

Fig. 5. Under reinforced T-beam. Crack patterns at various load levels up to failure for the mesh of 40 brick elements.

However, the beam continued to sustain load up to 195.84 kN, when the vertical crack in the top flange of the beam (half-way between the two load points) became visible. The relevant load–deflection curve, shown in Fig. 3, gave a considerably better prediction than those of the previous two runs; in fact, it compares reasonably well with the experimental limited-ductility curve, especially when one takes into consideration the numerically-indeterminate prediction between the MSL and the load at divergence (AFL in Fig. 3) [2].

The presence of the necessary transverse reinforcement in the region beyond the second load point seems to delay the formation of early vertical cracking in the flange and thus enables the attainment of a larger load-carrying capacity, consistent with the experimental evidence. Another possible reason for the improved prediction might be the adoption of larger elements in the longitudinal direction, moving the Gauss points away from the loading locations; thus the Gauss points become less stressed, avoiding the triggering of early failure. Finally, it is significant that an additional run using a 24-brick FE mesh, which does not contain the element representing the end block in the 25-brick mesh but is otherwise identical with the latter, predicted the MSL to be equal to 184.32 kN. This load being 6% less than the prediction of the present section, points to the effectiveness of incorporating the end block, an integral part of the specimen tested in the laboratory (and of good design practice), in the numerical analysis; such a structural measure delays early cracking in the support zone through which the compressive force passes. A further improvement in the overall prediction could probably be achieved by adopting the spacing of the web and flange reinforcement closer to the actual details of the experimental beam.

MODELLING OF HIGH-STRENGTH RC MEMBERS

Although the successful analysis of widely differing structural forms using the present FE model has been reported [1–3], all such case studies consisted of normal concrete-strength mixes. In fact, a shear wall failing in flexure, made from concrete with a cylinder compressive characteristic of $f_c = 44.2$ MPa, represents the upper bound of material strength beyond which the model has not yet been tested. Now, the constitutive relations for concrete under generalized states of stress have been the subject of extensive experimental research at Imperial College [9–13], the outcome of which is a stress–strain law [14] valid for concrete with an f_c up to at least 100 MPa. Since this general constitutive law has been incorporated into the present 3-D model, the study of high-strength concrete structures is within the capabilities of the FE package.

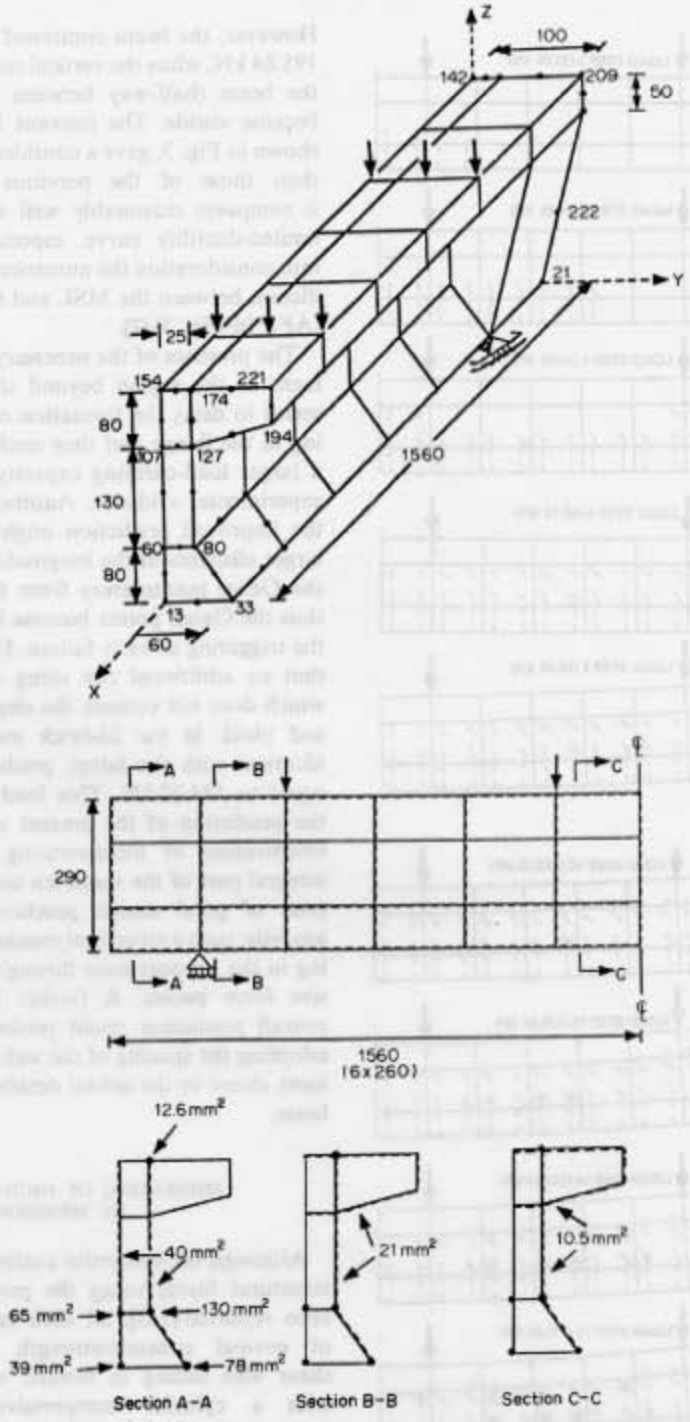

Fig. 6. Under-reinforced T-beam. Mesh of 25 brick elements. (Due to symmetry only one-fourth of the beam is analysed. The position of the steel elements is indicated by dashes.)

Case study 1: high-strength RC T-beam subjected to four-point loading failing in flexure

The beam HSB1 tested by Seraj [7] and made from a concrete with $f_c = 69.5$ MPa is analysed in this section. The beam is very much akin to the member used in the economic-modelling study (the latter being referred to as beam C in [8]). Thus, though the properties (i.e. strength and bar size) of the transverse reinforcement of HSB1 were slightly different from those of beam C, its arrangement was similar to that of the latter member. Figure 8 shows the details of the transverse-reinforcement distribution throughout beam HSB1.

The FE discretization adopted for the present analysis is shown in Fig. 9. The mesh has 25 HX20

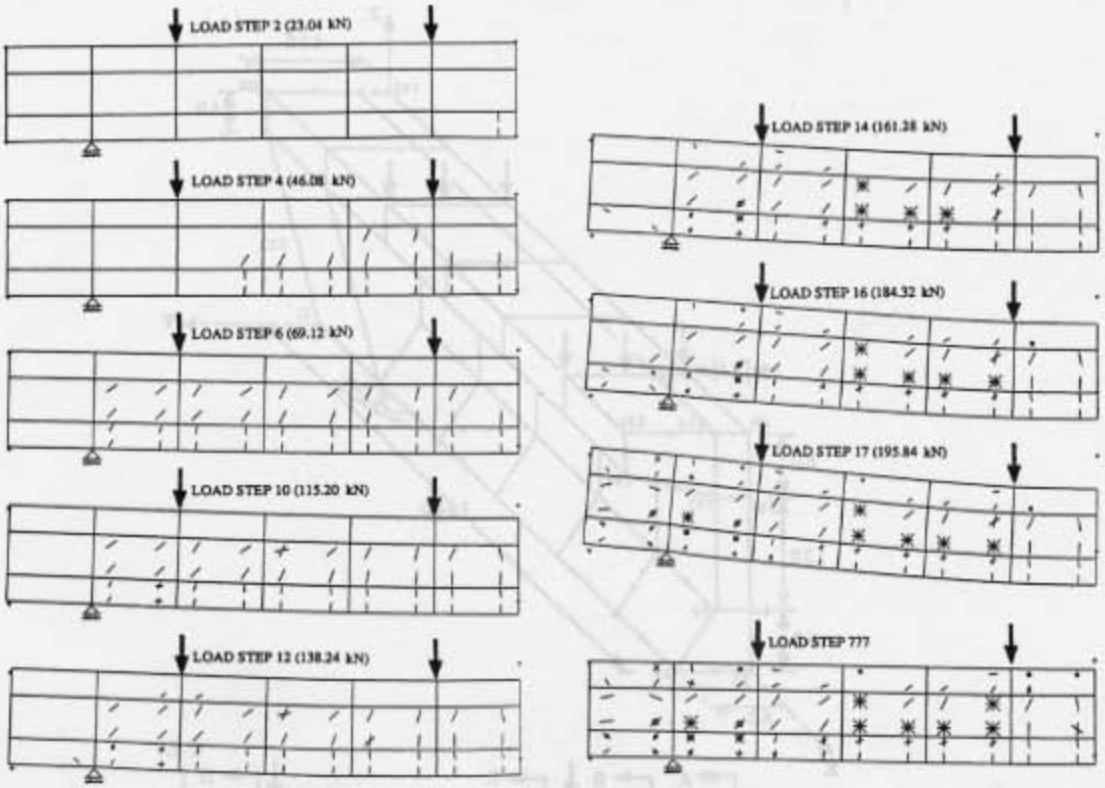

Fig. 7. Under-reinforced T-beam. Crack patterns at various load levels up to failure for the mesh of 25 brick elements. (Note: load step '777' not magnified.)

under-integrated brick elements for concrete and 82 LM03 bar elements for the steel (considering only one-fourth of the beam). The simplifications adopted are similar to those employed in the 25-brick mesh described earlier. In the present investigation, the yield and ultimate stress of the 1.5 mm ø steel were 460 and 510 MPa, respectively. For the 20 mm ø longitudinal bars, the yield and ultimate stress were 500 and 650 MPa, respectively.

The MSL in the analysis was 230.4 kN, which was about 1.5% above the experimental failure load (227 kN). However, a closer investigation of the loading configurations adopted in both analysis and experiment reveals that the FE modelling actually

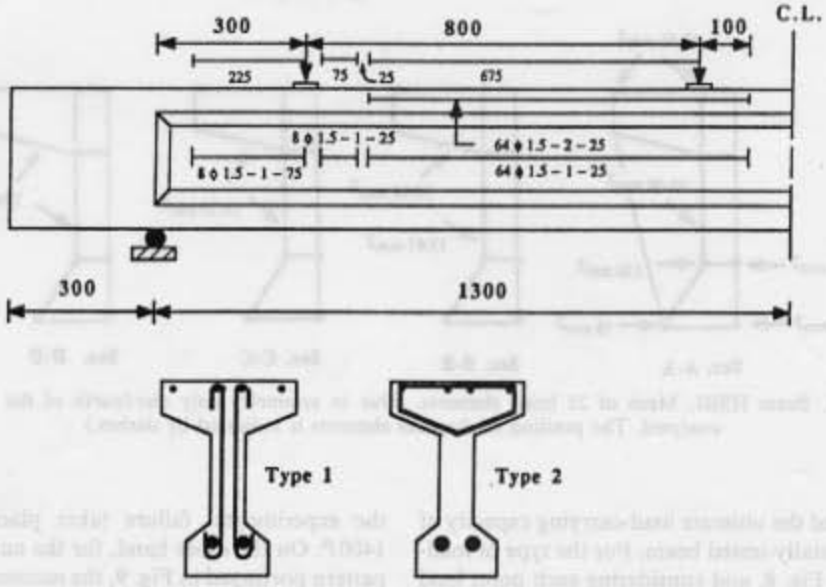

Fig. 8. Beam HSB1 [7]. Dimensions and reinforcement detailing.

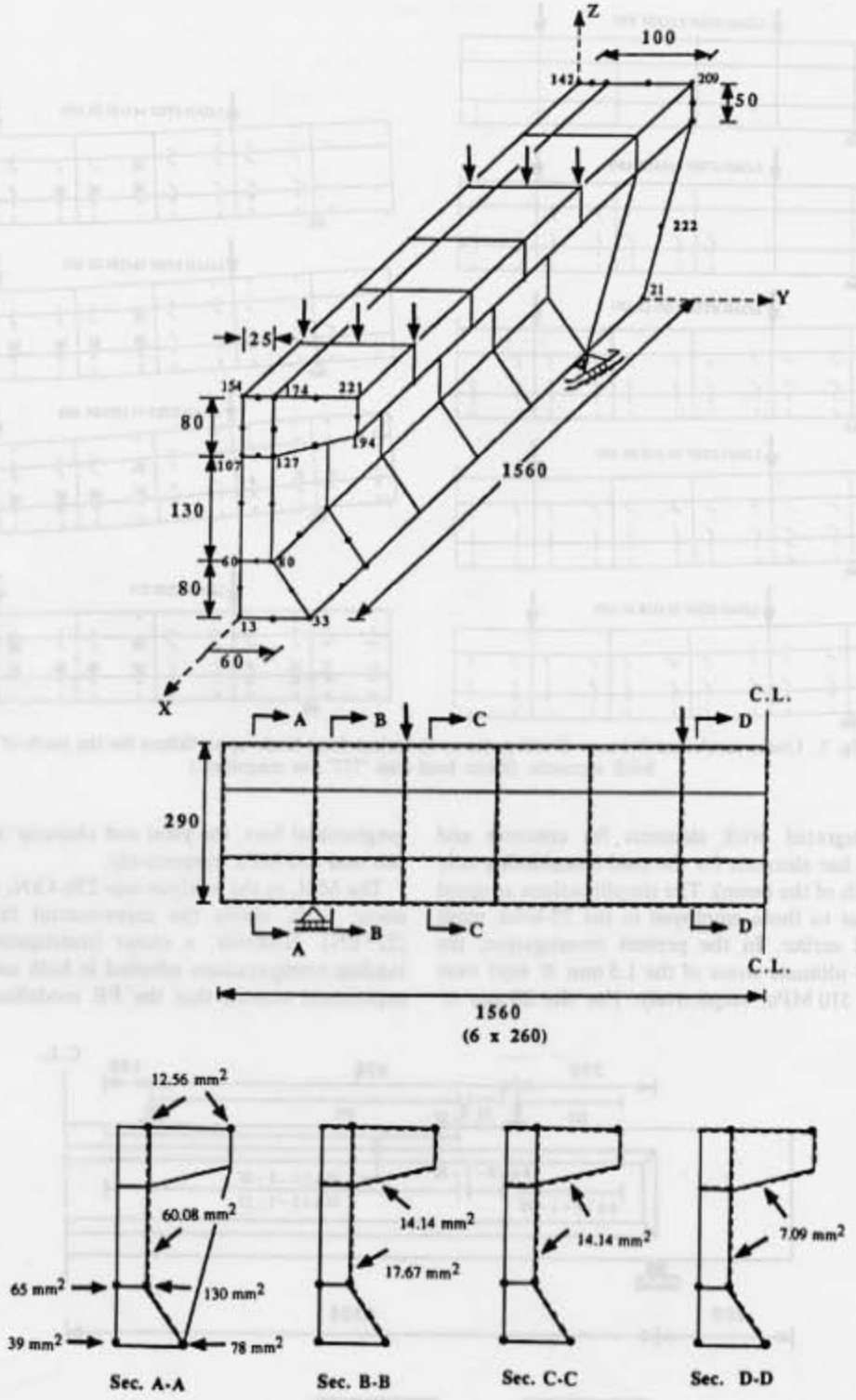

Fig. 9. Beam HSB1. Mesh of 25 brick elements. (Due to symmetry only one-fourth of the beam is analysed. The position of the steel elements is indicated by dashes.)

underpredicted the ultimate load-carrying capacity of the experimentally-tested beam. For the type of loading shown in Fig. 8, and considering each point load to be equal to P, the moment at mid-span, at which the experimental failure takes place, is equal to $1400P$. On the other hand, for the analytical loading pattern portrayed in Fig. 9, the moment at failure can be calculated to be equivalent to $1300P$. Thus the

analytical failure load should have been 7.7% higher than the experimental failure load, in order to attain the same flexural moment at failure. As such, the analytical prediction may be considered to be 6.2% lower than the actual experimental failure load. It is, however, important to note that, since HSB1 was designed in accordance to the compressive-force path concept [8], its transverse-reinforcement details were significantly different from current code requirements. It contained a very low amount of web reinforcement. As a result, the failure load of HSB1, according to the British Code, should have been 46.74 kN [7] and the member should have undergone a shear failure. Although the location of the point loads had to be slightly altered in order to adopt a regular mesh in the analysis [which resulted in a slight reduction in the amount of flexural stresses at different sections (of the order of 13/14 in the flexural span)], the shear forces acting at critical portions of the beam were unaffected. Thus, the beam under investigation did, in fact, sustain practically the same shear forces at critical sections, both in the experiment and in this FE analysis.

Figure 10 shows the analytical crack patterns at various load levels up to failure. At 46.08 kN, the first set of flexural cracks appeared within the flexural span and below the inner load points. In subsequent load steps, new flexural cracks formed near the mid-span, while existing cracks propagated upwards. At a load of 92.16 kN, diagonal cracks oriented from the supports to the point loads developed throughout the web of the beam. The top flange remained uncracked until the load reached the value of 149.76 kN, when an inclined crack penetrated into the bottom part of the compression flange. At 195.84 kN, more inclined cracks were formed below the load points. In this and in the following load steps, the web in between the load points in the shear span was severely cracked. Upon reaching the MSL level, horizontal cracks at the top of the flange could be seen. In Fig. 11, the applied load is plotted against the mid-span deflection, the close agreement between

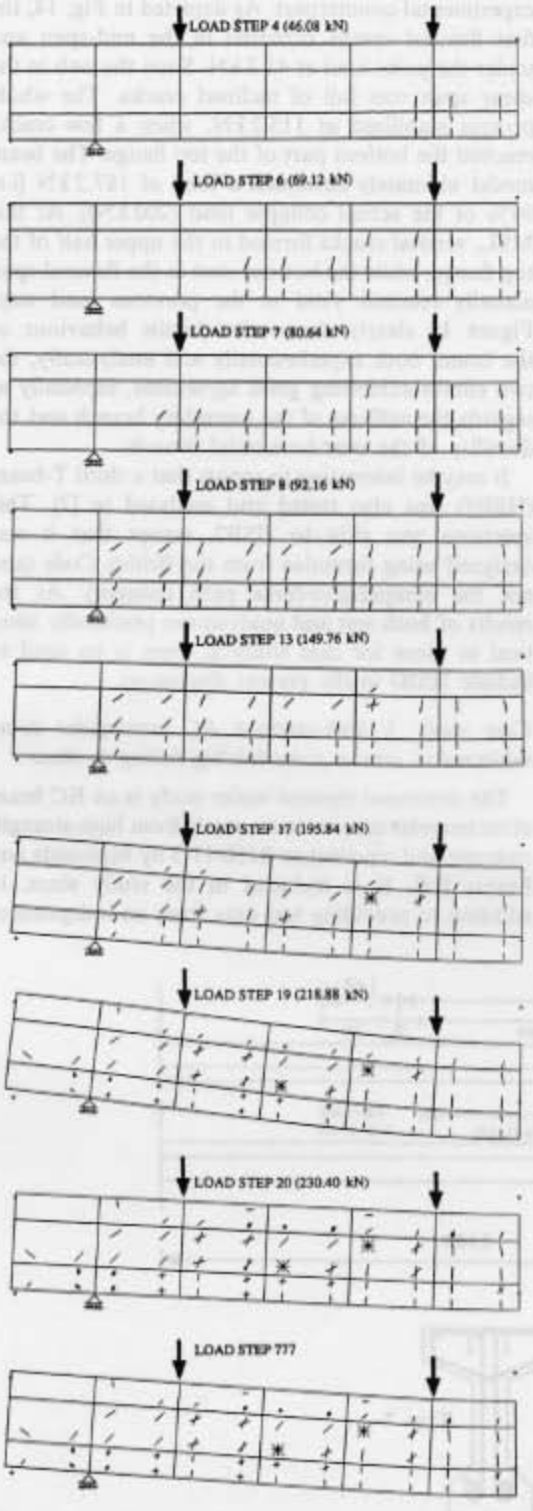

Fig. 10. Beam HSB1. Crack patterns at various load levels up to failure. (Note: load steps 20 and '777' not magnified.)

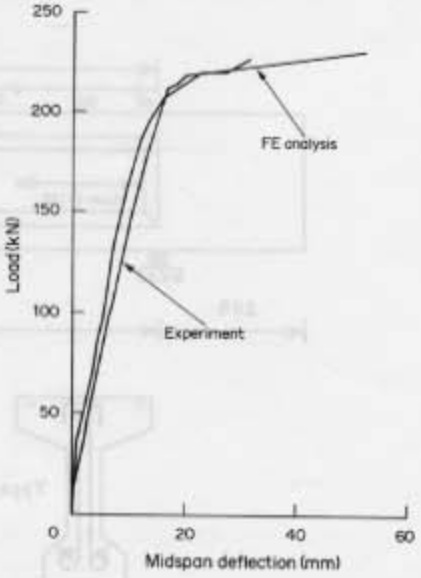

Fig. 11. Beam HSB1. Comparison between experimental and analytical load–deflection curves.

experiment and analysis being apparent. The nature of the experimental curve points to flexural failure of the beam, although the ductility is somewhat limited. On the other hand, the total amount of deflection at failure (i.e. MSL) is overestimated in the FE prediction. It is apparent from the above analytical excerise that the load-carrying capacity, cracking process and deformational response have been closely simulated by the adopted FE model.

Case study 2: high-strength RC T-beam subjected to two-point loading failing in flexure

This beam (HSB2) is identical in size and sectional characteristics to the high-strength member studied in the previous section. However, the present under-reinforced T-beam was loaded by two-point loading with a shear span of 800 mm and a flexural span of 1000 mm, the flexural capacity being 78.64 kN m. The experimental details of beam HSB2, designed in accordance to the compressive-force path concept [8], are available elsewhere [7]. The member was made from a concrete with $f_c = 70.2$ MPa. Figure 12 shows details of the transverse reinforcement distribution of the beam. The FE discretization is similar to the one adopted for the analysis of HSB1 (case study 1). Details of the mesh (consisting of 25 brick and 74 bar elements) and the position and amount of the steel are given in Fig. 13. Though the longitudinal and transverse steel had to be 'smeared' to its adjoining nodes in a manner similar to the earlier analyses, the length of the shear span in the present analysis was equal to its actual experimental value; this gave rise to identical moments and shear forces at all sections, both in the experiment and in the FE analysis. However, the flexural span was 1040 instead of 1000 mm; nevertheless, this deviation is of minor consequence. In the analysis of HSB2, the yield stress and the ultimate stress of the 6 mm ø transverse reinforcement was taken as 570 and 665 MPa, respectively.

The analytical findings can be seen by reference to Figs 14 and 15, which give, respectively, crack patterns at various load levels up to failure and a comparison of the load–deflection curve with its experimental counterpart. As depicted in Fig. 14, the first flexural cracks occurred in the mid-span and under the point load at 43.2 kN. Soon the web in the shear span was full of inclined cracks. The whole process stabilized at 115.2 kN, when a few cracks reached the bottom part of the top flange. The beam model ultimately sustained a load of 187.2 kN [i.e. 94% of the actual collapse load (200 kN)]. At this MSL, vertical cracks formed in the upper half of the top flange, while the bottom steel in the flexural span actually reached yield in the previous load step. Figure 15 clearly shows the ductile behaviour of the beam, both experimentally and analytically, the two curves exhibiting good agreement, especially as regards the stiffness of the ascending branch and the ductility of the near-horizontal branch.

It may be interesting to report that a third T-beam (HSB3) was also tested and analysed in [7]. This specimen was akin to HSB2, except that it was designed using formulae from the British Code (and not the compressive-force path concept). As the results of both test and analysis are practically identical to those for case study 2, there is no need to include HSB3 in the present discussion.

Case study 3: high-strength RC rectangular beam subjected to central point loading failing in shear

The structural element under study is an RC beam of rectangular cross-section, made from high-strength concrete and reported as B150-11-3 by Mphonde and Frantz [15]. It is included in the study since, in addition to providing test data from an independent

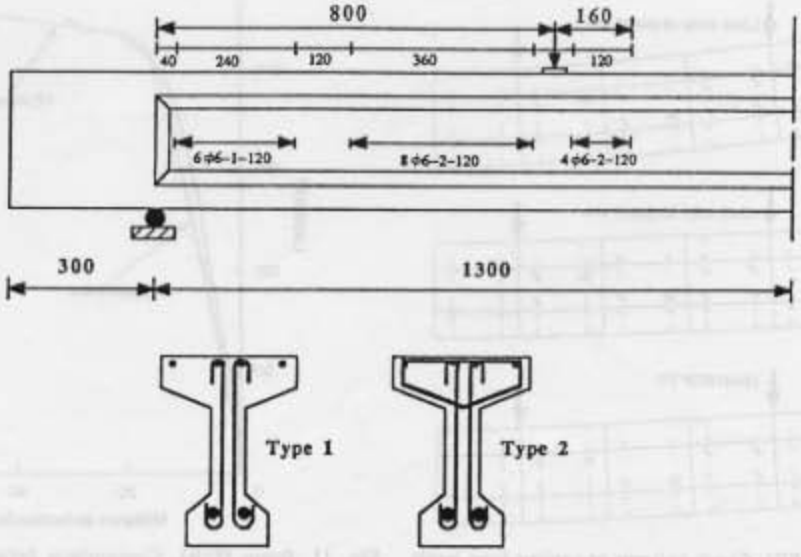

Fig. 12. Beam HSB2 [7]. Dimensions and reinforcement detailing.

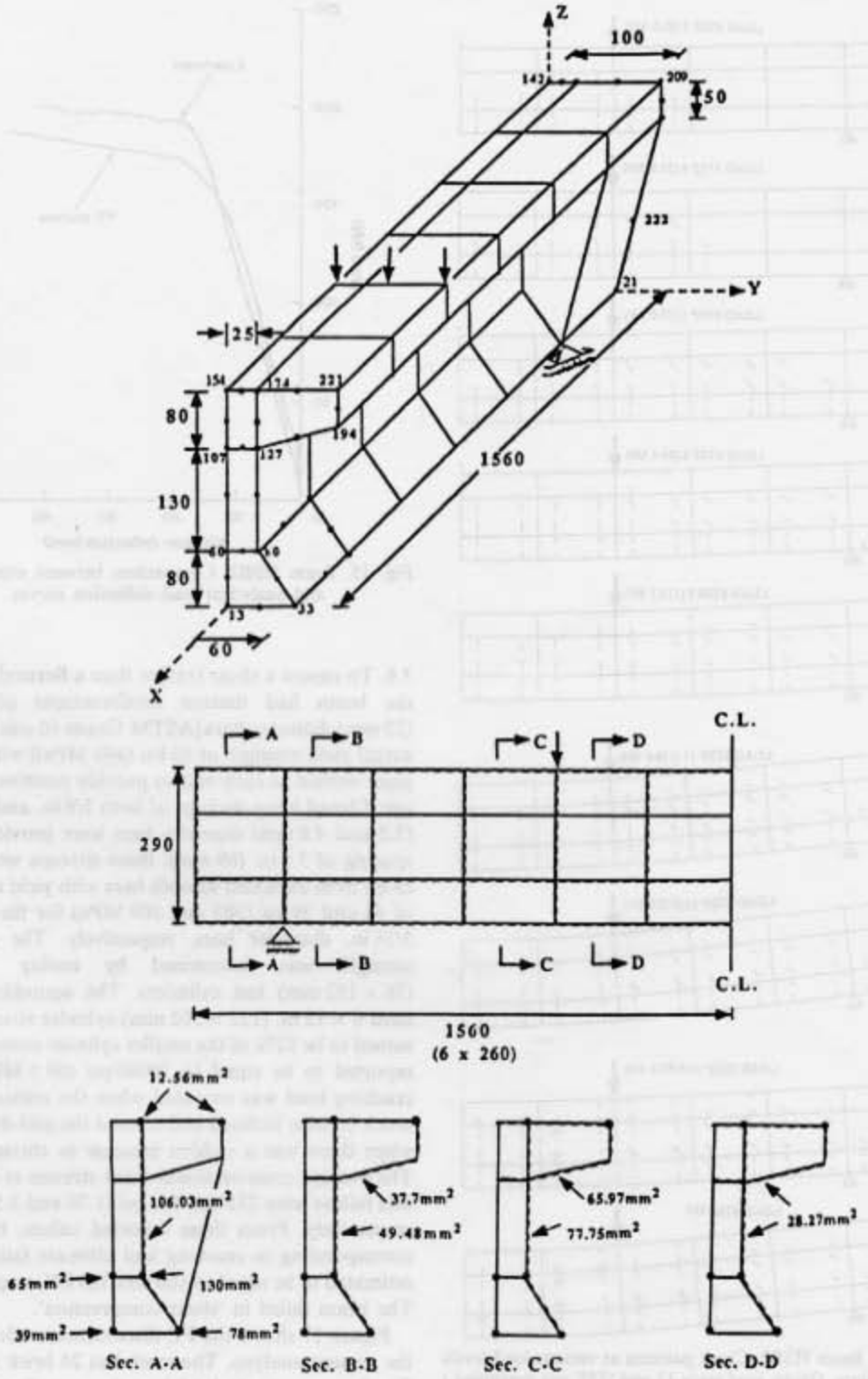

Fig. 13. Beam HSB2. Mesh of 25 brick elements. (Due to symmetry only one-fourth of the beam is analysed. The position of the steel elements is indicated by dashes.)

laboratory (such data being relatively scarce for high-strength concrete members), it refers to the more standard rectangular shape of cross-section—providing what appears to be one of the first attempts to model numerically a high-strength beam of this basic form.

The details of the experimental beam and the typical crack patterns at failure are given in Fig. 16.

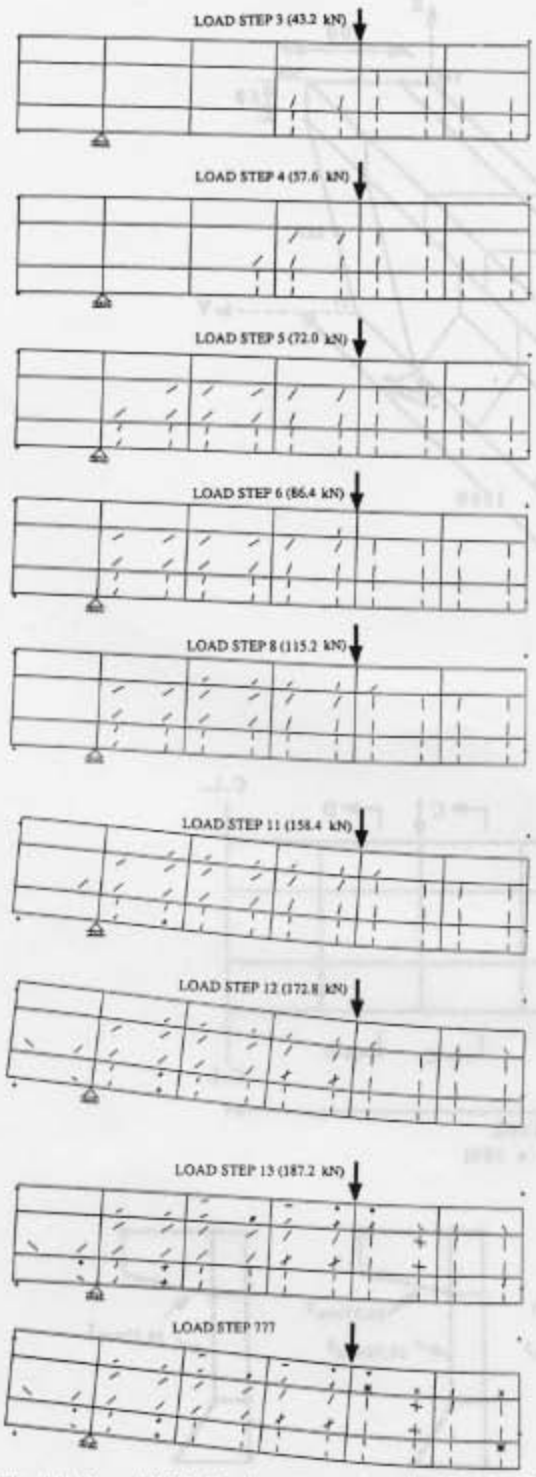

Fig. 14. Beam HSB2. Crack patterns at various load levels up to failure. (Note: load steps 13 and '777' not magnified.)

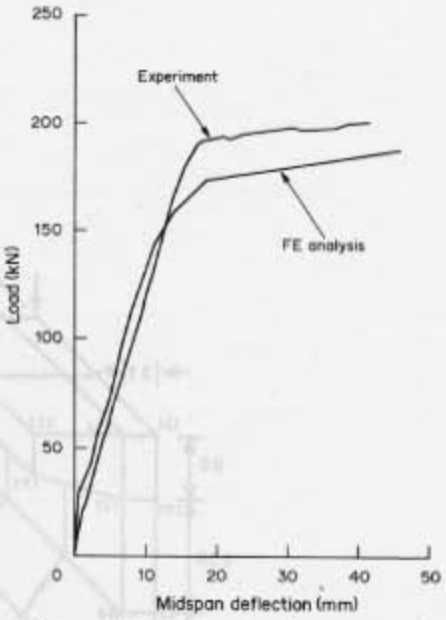

Fig. 15. Beam HSB2. Comparison between experimental and analytical load–deflection curves.

As indicated in Fig. 16(a), the beam was $6 \times 13.25 \times 96$ in. ($152 \times 337 \times 2438$ mm) with an effective depth of 11.75 in. (298 mm) and a cover of 1 in. (25 mm). It was simply supported, being loaded at mid-span to produce a shear span-to-depth ratio of 3.6. To ensure a shear (rather than a flexural) failure, the beam had tension reinforcement of 3–1 in. (25 mm) diameter bars [ASTM Grade 60 steel with an actual yield strength of 65 ksi (448 MPa)] with a steel plate welded at each end to provide positive anchorage. Closed hoop stirrups of both 1/8 in. and 3/16 in. (3.2 and 4.8 mm) diameter bars were provided, at a spacing of 3.5 in. (89 mm); these stirrups were fabricated from annealed smooth bars with yield strengths of 44 and 39 ksi (303 and 269 MPa) for the 1/8 and 3/16 in. diameter bars, respectively. The concrete strength was determined by testing 3×6 in. (76×152 mm) test cylinders. The equivalent standard 6×12 in. (152×305 mm) cylinder strength, assumed to be 92% of the smaller cylinder strength, was reported to be equal to 10080 psi (69.5 MPa). The cracking load was recorded when the critical failure crack became inclined and crossed the mid-depth and when there was a sudden increase in stirrup strain. The average cross-sectional shear stresses at cracking and failure were 255 and 515 psi (1.76 and 3.55 MPa), respectively. From these reported values, the loads corresponding to cracking and ultimate failure were estimated to be equal to 160 and 323 kN, respectively. The beam failed in 'shear compression'.

Figure 17 shows the FE discretization adopted for the present analysis. The mesh has 24 brick elements for the concrete and 64 bar elements for the steel (with reference to the one-fourth of the beam that was analysed). The reinforcement area for the various steel elements of the mesh is also indicated in Fig. 17. The tension reinforcement was concentrated at a distance from the top face equal to the effective depth of the beam and the concrete cover was neglected altogether; in this respect, the adopted mesh is

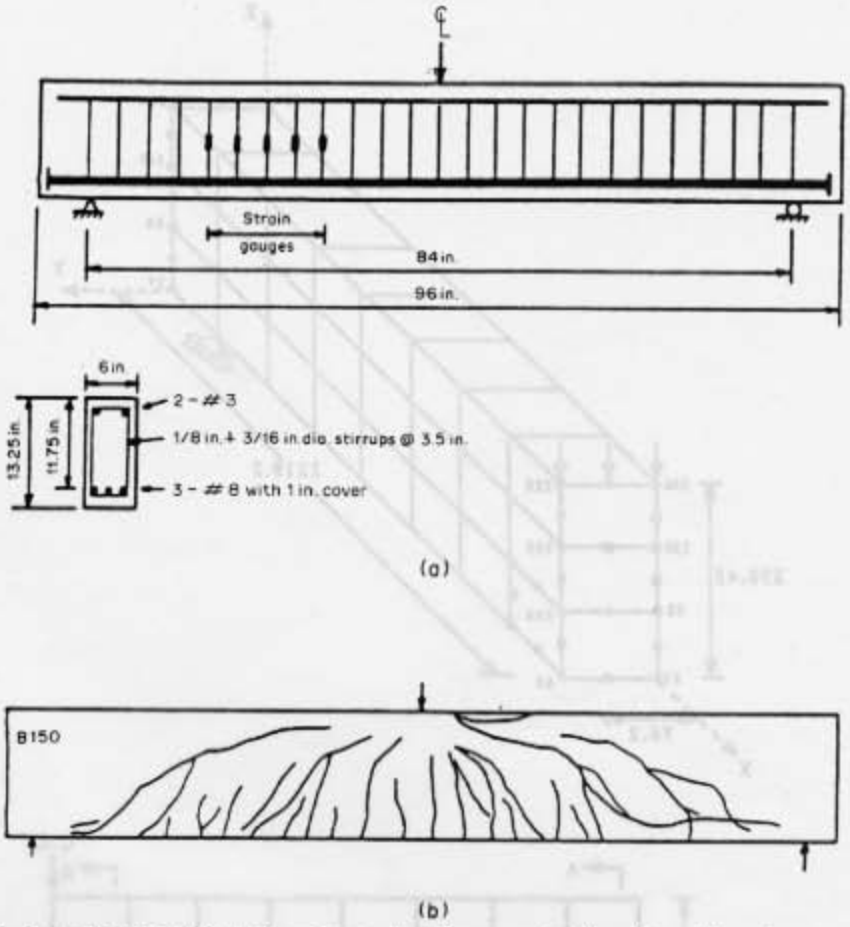

Fig. 16. Beam B150-11-3 [15]: (a) dimensions and reinforcement detailing; (b) typical crack pattern after failure.

compatible with the minor contribution of the cracked areas to the transfer of shear forces [16], and, thus, it appears that neglecting the cover can only affect the deformational response of the beam, while the ultimate-load prediction is insenstive to such a simplification [6]. The compression reinforcement was 'smeared' to the top edge of the beam; again, this modification is unlikely to affect results. While the spacing of the stirrups in the test was 88.9 mm, that in the model was 152.4 mm; thus the area of transverse reinforcement had to be adjusted so as to have the same stirrup shear capacity. Though both 303 and 269 MPa yield-strength stirrups were used in the test at the same location, only the 269 MPa stirrups were adopted for the analysis, in order to minimize the number of bar elements; however, the overall stirrup shear capacity was kept at the required value.

The MSL in the analysis was 360 kN, which is 11% above the experimental failure load. Figure 18 shows the analytical crack patterns at various load steps up to failure. At 72 kN, the first vertical flexural cracks were observed in the middle part of the beam. With the increase in load, the cracks followed curved paths in the direction of increasing moment towards the compression zone. The crack propagation was almost stabilized from 270 kN until 324 kN, when a large number of near-horizontal cracks suddenly appeared in the top one-third, i.e. in the compression zone of the beam; although these cracks reached the vicinity of the load point, their propagation through the compression zone was arrested. Subsequently, the beam sustained some further load without much additional cracking. At the MSL of 360 kN, the extension of the more severe crack from the top surface of the beam towards the support through the compression zone of the beam is detectable through the new cracks formed under the load and at the support. Eventually, 'shear' failure took place. The analytical crack pattern at the MSL (load step 20 in Fig. 18) resembles well its experimental counterpart (Fig. 16b). Stresses in both the longitudinal and transverse steel were below their yield limits at failure (i.e. load step 20). Finally, Fig. 19 shows the relevant load-deflection curves. It may be seen that both the experimental characteristic and the analytical prediction are in excellent agreement up to about 200 kN. However, beyond this load, the latter becomes stiffer. Now, the model used in the analysis relies greatly on the material properties. In this respect, it has already been pointed out that, in the absence of actual values

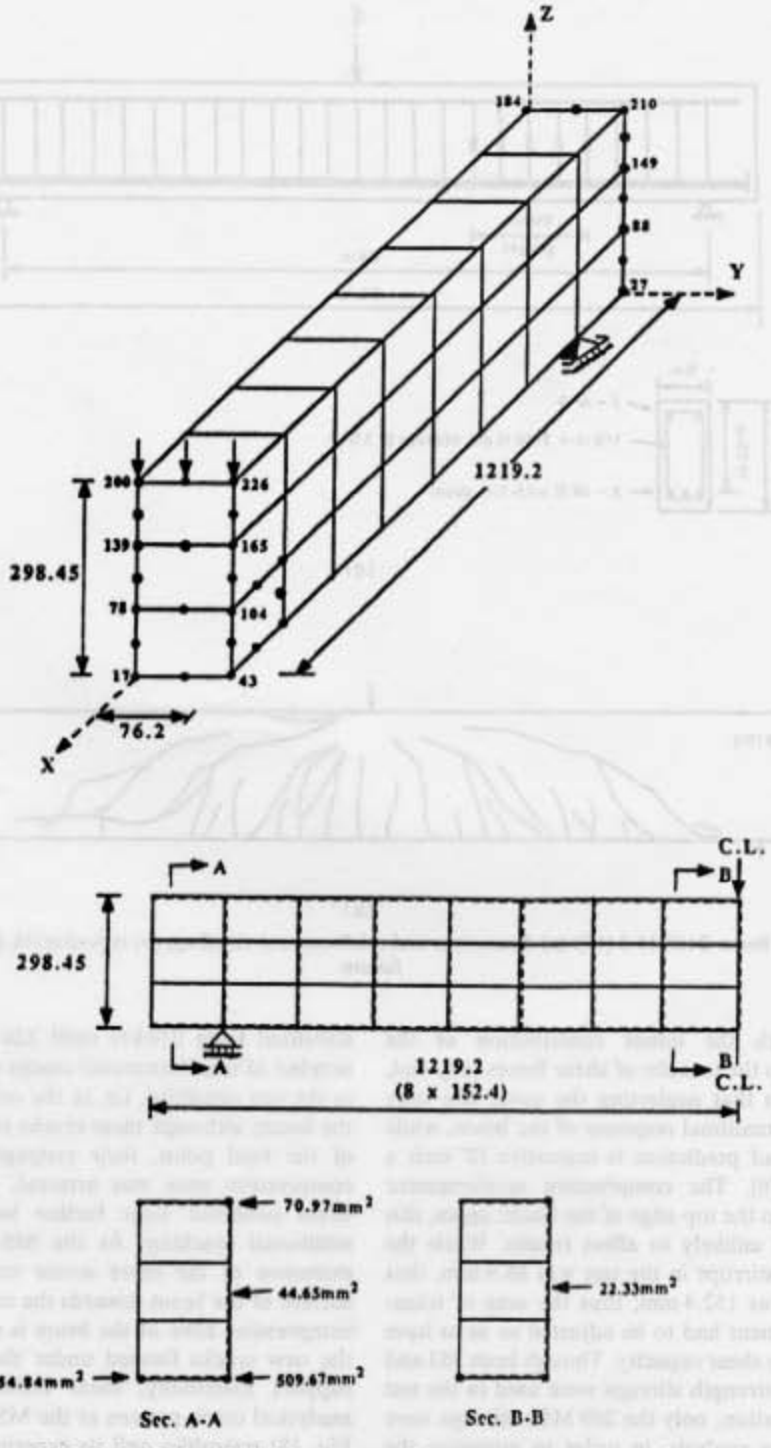

Fig. 17. Beam B150-11-3. Mesh of 24 brick elements. (Due to symmetry only one-fourth of the beam is analysed. The position of the steel elements is indicated by dashes.)

of standard cylinder compressive strength, the value of f_c was estimated from 76.2 × 152.4 mm cylinder strengths. But such an estimated f_c reported by the investigators [15] is applicable to the American standard cylinder having size 6 × 12 in. On the other hand, the input for f_c used in the FE model is based on the British standard cylinder having size 100 × 250 mm (4 × 10 in.). Now, it is known that, for an increase in the height/diameter ratio from 2 to 2.5, the f_c value of normal-strength concrete can decrease by about 10% [17]. This reduction in f_c, though less pronounced in high-strength concretes, if considered in the input of the FE model, would have certainly closed the gap between the analytical and

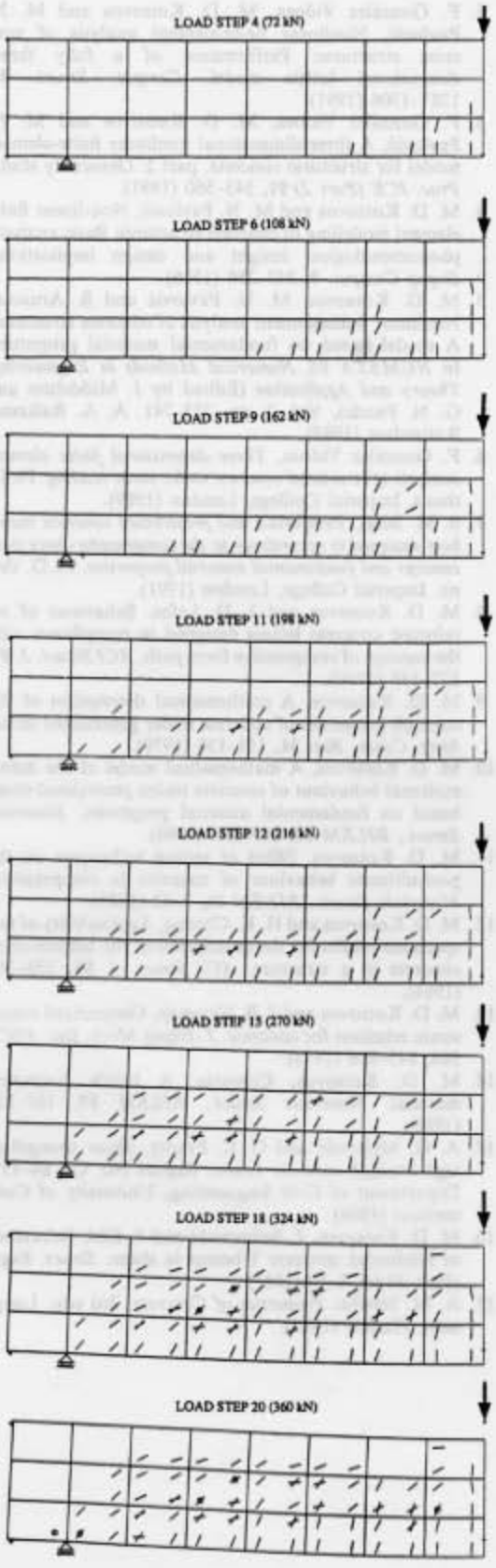

Fig. 18. Beam B150-11-3. Crack patterns at various load levels up to failure.

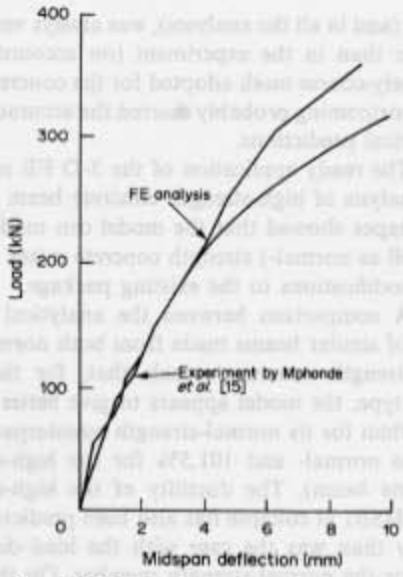

Fig. 19. Beam B150-11-3. Comparison between experimental and analytical load–deflection curves.

experimental failure loads for this case study. Also, the actual stress–strain curve of the reinforcing steel was not available; hence, the ultimate strength was assumed to be 15% higher than the yield strength. Nevertheless, despite these uncertainties, it appears that the present model simulates quite well the overall behaviour of a structural element with rectangular cross-section made from high-strength concrete.

CONCLUSIONS

The present study based on the 3-D FE model for structural concrete described in [1–3], leads to the following main conclusions:

1. It is evident from the exercise of modelling the same structural form using simpler FE discretizations that the behaviour of RC structures can be simulated numerically in a satisfactory manner even with coarse FE meshes, provided that all the structurally-significant features pertaining to geometry and reinforcement arrangement are incorporated—albeit approximately—in the analysis. Thus, mesh refinement need not be a precondition in accomplishing faithful prognoses from a FE model for structural concrete that is based on a proper understanding of the properties at the material level. It is worth recalling that the beam used in the preliminary economic-modelling study had a complicated geometry and elaborate reinforcement detailing. A 10% improvement in its ultimate failure-load prediction was achieved by better detailing of the flange reinforcement and the introduction of the concrete end block. In fact, the inclusion of the rectangular end block in the FE discretization alone improved the prediction by about 6%. On the other hand, the spacing of the transverse reinforcement, both in the web and in the

flange (and in all the analyses), was always very much greater than in the experiment (on account of the relatively-coarse mesh adopted for the concrete), and this shortcoming probably marred the accuracy of the numerical predictions.

2. The ready application of the 3-D FE model to the analysis of high-strength concrete beam of various shapes showed that the model can model high- (as well as normal-) strength concrete mixes without any modifications to the existing package.

3. A comparison between the analytical predictions of similar beams made from both normal- and high-strength concrete reveals that, for the latter beam type, the model appears to give better predictions than for its normal-strength counterpart (82% for the normal- and 101.5% for the high-strength concrete beam). The ductility of the high-strength beam HSB1 at collapse has also been predicted more readily than was the case with the load–deflection plot for the normal-strength member. On the other hand, the limited ductility of the quasi-ductile beam made from normal-strength concrete could not be predicted so precisely by the FE discretization adopted. Now, the role of flange reinforcement in achieving ductility in a normal-strength concrete beam was demonstrated in [8]. In contrast, a recent investigation [7] has shown that the role of similar reinforcement towards the ductile behaviour of high-strength concrete beams is of less importance. Therefore, while the over-simplified modelling of flange reinforcement in HSB1 did not show much adverse effect on the prediction, it did affect the prediction of beam C at loads near failure, where flange reinforcement plays an active part. On the basis of such findings—admittedly derived from the present limited analytical data—it would appear that a tentative conclusion might be that less attention need be payed to the FE discretization of the reinforcement in the case of high-strength members. For, unlike their normal-strength counterparts, such components are known to exhibit less triaxial effects near failure and, hence, are less dependent on the actual confinement provided by the reinforcing steel.

REFERENCES

1. F. González Vidosa, M. D. Kotsovos and M. N. Pavlović, A three-dimensional nonlinear finite element model for structural concrete. Part 1: Main features and objectivity study. *Proc. ICE (Part 2)* **91,** 517–544 (1991).
2. F. González Vidosa, M. D. Kotsovos and M. N. Pavlović, Nonlinear finite-element analysis of concrete structures: Performance of a fully three-dimensional brittle model. *Comput. Struct.* **40,** 1287–1306 (1991).
3. F. González Vidosa, M. D. Kotsovos and M. N. Pavlović, A three-dimensional nonlinear finite-element model for structural concrete. part 2: Generality study. *Proc. ICE (Part 2)* **91,** 545–560 (1991).
4. M. D. Kotsovos and M. N. Pavlović, Non-linear finite element modelling of concrete structures: Basic analysis, phenomenological insight and design implications. *Engng Comput.* **3,** 243–250 (1986).
5. M. D. Kotsovos, M. N. Pavlović and S. Arnaout, Nonlinear finite element analysis of concrete structures: A model based on fundamental material properties. In *NUMETA 85, Numerical Methods in Engineering: Theory and Application* (Edited by J. Middelton and G. N. Pande), Vol. 2, pp. 733–741. A. A. Balkema, Rotterdam (1985).
6. F. González Vidosa, *Three-dimensional finite element analysis of structural concrete under static loading*. Ph.D. thesis. Imperial Coillege, London (1989).
7. S. M. Seraj, *Reinforced and prestressed concrete members designed in accordance to the compressive-force path concept and fundamental material properties*. Ph.D. thesis. Imperial College, London (1991).
8. M. D. Kotsovos and I. D. Lefas. Behaviour of reinforced concrete beams designed in compliance with the concept of compressive force path. *ACI Struct. J.* **87,** 127–139 (1990).
9. M. D. Kotsovos, A mathematical description of the strength properties of concrete under generalized stress. *Mag. Concr. Res.* **31,** 151–158 (1979).
10. M. D. Kotsovos, A mathematical model of the deformational behaviour of concrete under generalized stress based on fundamental material properties. *Materials Struct., RILEM* **13,** 289–298 (1980).
11. M. D. Kotsovos, Effect of testing techniques on the post-ultimate behaviour of concrete in compression. *Materials Struct., RILEM* **16,** 3–12 (1983).
12. M. D. Kotsovos and H. K. Cheong, Applicability of test specimen results for the description of the behaviour of concrete in a structure. *ACI Struct. J.* **81,** 358–363 (1984).
13. M. D. Kotsovos and J. B. Newman, Generalized stress-strain relations for concrete. *J. Engng Mech. Div. ASCE* **104,** 845–856 (1978).
14. M. D. Kotsovos, Concrete. A brittle fracturing material. *Materials Struct., RILEM* **17,** 107–115 (1984).
15. A. G. Mphonde and G. C. Frantz, *Shear strength of high strength concrete beams*. Report No. CE 84-157, Department of Civil Engineering, University of Connecticut (1984).
16. M. D. Kotsovos, J. Bobrowski and J. Eibl, Behaviour of reinforced concrete T-beams in shear. *Struct. Engr. (Part B)* **65,** 1–10 (1987).
17. A. M. Neville. *Properties of Concrete*, 3rd edn. Longman, Harlow (1981).